Title
CAPE Times P Explains Lightning Over Land But Not the Land-Ocean Contrast

Journal
Geophysical Research Letters, 45(22)

ISSN
0094-8276

Authors
Romps, DM
Charn, AB
Holzworth, RH
et al.

Publication Date
2018-11-28

DOI
10.1029/2018GL080267

Peer reviewed

CAPE Times P Explains Lightning Over Land But Not the Land-Ocean Contrast

David M. Romps[1,2], Alexander B. Charn[1], Robert H. Holzworth[3], William E. Lawrence[4], John Molinari[5], and David Vollaro[5]

[1]Department of Earth and Planetary Science, University of California, Berkeley, CA, USA, [2]Climate and Ecosystem Sciences Division, Lawrence Berkeley National Laboratory, Berkeley, CA, USA, [3]Department of Earth and Space Sciences, University of Washington, Seattle, WA, USA, [4]National Weather Service Arkansas-Red Basin River Forecast Center, National Weather Service, Tulsa, OK, USA, [5]Department of Atmospheric and Environmental Sciences, State University of New York at Albany, Albany, NY, USA

Correspondence to: D. M. Romps, romps@berkeley.edu

Abstract

The contemporaneous pointwise product of convective available potential energy (CAPE) and precipitation is shown to be a good proxy for lightning. In particular, the CAPE × P proxy for lightning faithfully replicates seasonal maps of lightning over the contiguous United States, as well as the shape, amplitude, and timing of the diurnal cycle in lightning. Globally, CAPE × P correctly predicts the distribution of flash rate densities over land, but it does not predict the pronounced land-ocean contrast in flash rate density; some factor other than CAPE or P is responsible for that land-ocean contrast.

Plain Language Summary

Forecasting lightning is a challenge because weather and climate models do not resolve the processes that lead to the electrification of clouds. Instead, simple models must be used to predict lightning based on the available data. One model that has been proposed is the product of convective available potential energy, which is a measure of potential storm energy, times the precipitation rate. It is shown here that convective available potential energy times the precipitation rate explains the distribution and timing of lightning over land but does not explain the large land-ocean contrast in lightning flash rates.

1 Introduction

Weather and climate models do not simulate lightning explicitly. Therefore, to generate a lightning forecast, a parameterization or proxy for lightning must be used. Romps et al. (2014, hereafter, R14) argued that the product of convective available potential energy (CAPE) and precipitation, written as CAPE × P, should be a faithful proxy for lightning. The empirical evidence presented by R14, however, consisted primarily of a comparison of time series integrated over the contiguous United States (CONUS) at 12-hourly resolution over a single year. In particular, R14 showed that, during the 2011 calendar year, the 12-hourly time series of $\langle \mathrm{CAPE} \rangle \times \langle P \rangle$ (where angle brackets denote a spatial average over CONUS) explains 77% of the variance in $\langle F \rangle$ (where F is the cloud-to-ground lightning flash rate).

Although this is an impressive fraction of variance explained, the reliance on CONUS-integrated values and 12-hr times steps leaves many questions unanswered. For example, R14 did not address whether CAPE × P can predict the spatial distribution or diurnal cycle of lightning flashes. Nor did R14 explore whether CAPE × P could explain the order-of-magnitude larger rate of lightning over land compared to the ocean. Although mean CAPE values are relatively similar over the land and ocean (Lucas et al., 1994), it is plausible that transiently high values of CAPE (made possible over land by the surface's low heat capacity) could give rise to large mean values of CAPE × P over land and, therefore, explain the land-ocean lightning contrast.

Here we use a variety of observational data sets to assess the spatial and temporal performance of the CAPE × P proxy in far more detail than in R14. In particular, the validation is extended to CONUS seasonal maps, the CONUS diurnal cycle, and the global distribution. For these analyses, we use four data sets of observed CAPE, four data sets of observed precipitation, and three data sets of observed lightning.

2 Data Sources

The data sources for CAPE, precipitation, and lightning are summarized in Table 1. CAPE values are calculated (using conservation of MSE-CAPE; Romps, 2015; Romps & Kuang, 2010) from the radiosonde profiles of the National Weather Service Radiosonde Replacement System (RRS; NCDC, 2008) and also taken from the output of three reanalyses: the National Centers for Environmental Prediction (NCEP) North American Regional Reanalysis (NARR; Mesinger et al., 2006), the European Centre for Medium-Range Weather Forecasts (ECMWF) re-analysis referred to as ERA-Interim (ERA; Dee et al., 2011), and the twentieth Century Reanalysis version 2 (20CRv2) using the NCEP atmosphere-land model (20CR; Compo et al., 2011). The precipitation data are taken from the same three reanalyses and also from the National Weather Service River Forecast Centers (RFC; Kitzmiller et al., 2013). For lightning, the data come from the National Lightning Detection Network (NLDN; Cummins & Murphy, 2009; Orville & Huffines, 2001; Wacker & Orville, 1999), the World Wide Lightning Location Network (WWLLN; Hutchins et al., 2012; Jacobson et al., 2006; Virts et al., 2013), and a merged climatology from the Lightning Imaging Sensor and the Optical Transient Detector (LIS-OTD; Cecil et al., 2014; Mach et al., 2007). Further details on the data sources, their normalization, and their regridding are given in Text S1 in the supporting information.

Table 1
The Data Sources for CAPE, Precipitation, and Lightning

	Source	Keyword	Resolution	Frequency	Begin	End
CAPE	NARR	cape	~0.25°	3 hr	2005	2015
	ERA	cape	0.75°	3 hr	2005	2015
	20CR	cape	2°	6 hr	2005	2014
	RRS	7Lvls	~3°	12 hr	2010	2015
Precipitation	NARR	acpcp	~0.25°	3 hr	2005	2015
	ERA	precip	0.75°	3 hr	2005	2015
	20CR	cprat	~2°	3 hr	2005	2014
	RFC	rxmrg	~0.03°	1 hr	2010	2015
Lightning	NLDN		0.001°	1 s	2005	2015
	WWLLN	ltg_annual_hd_de	0.5°	Annual mean	2008	2013
	LIS-OTD	HRFC_V2.3.2014	0.5°	Annual mean	1998	2010

Note. Keyword specifies the variable name or the particular version of the data set. *Resolution* and *Frequency* refer to the native resolution and frequency of the data. *Begin* and *End* give the range of years that were available for this study (from 1 January of the beginning year to 31 December of the ending year). CAPE = convective available potential energy; NARR = North American Regional Reanalysis; ERA = ERA-Interim; 20CR = twentieth Century Reanalysis version 2; RRS = Radiosonde Replacement System; RFC = River Forecast Centers; NLDN = National Lightning Detection Network; WWLLN = World Wide Lightning Location Network; LIS-OTD = Lightning Imaging Sensor and the Optical Transient Detector.

3 Optimal Lag Between CAPE and P

Because CAPE can be reduced by precipitation-driven downdrafts, we may not want to use contemporaneous CAPE and P in the CAPE × P proxy. Instead, we may want to evaluate CAPE some time before the precipitation to get an accurate measure of the CAPE on which convection is feeding. To test this, we use NARR CAPE and NARR P over CONUS for 1 January 2010 to 31 December 2015 and calculate the R^2 between the 3-D NLDN cloud-to-ground lightning flashes F (the three dimensions are longitude, latitude, and time) and the 3-D CAPE × P values, all on NARR's 0.25°, 3-hourly grid. The left panel of Figure 1 shows the resulting R^2 as a function of the lag used for CAPE relative to P and F (see Text S2). The first thing to notice is that the R^2 values are all quite low: less than 20%. This is to be expected because these R^2 are calculated from 3-D data at relatively high spatial and temporal resolution, and lightning is random: flashes will correlate with instantaneous CAPE × P but not perfectly due to their stochastic nature.

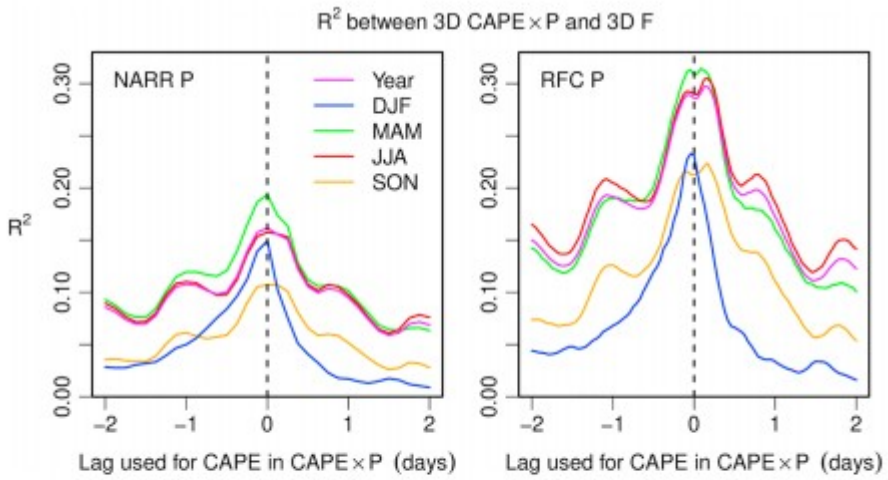

Figure 1. R^2 between 3-D CAPE × P and 3-D cloud-to-ground lightning flashes F using NLDN F and (left) NARR CAPE and NARR P or (right) NARR CAPE and RFC P. CAPE = convective available potential energy; NLDN = National Lightning Detection Network; NARR = North American Regional Reanalysis; RFC = River Forecast Centers. DJF = December, January, February; MAM = March, April, May; JJA = June, July, August; SON = September, October, November.

The next thing to notice is that the highest R^2 is achieved for zero lag, regardless of the season. This means that there is nothing to be gained by measuring CAPE at some time before or after the actual precipitation event: the best option is to simply use contemporaneous values. To test the robustness of this result, we repeat the analysis using NARR CAPE and RFC P, as shown in the right panel of Figure 1, now making hourly maps by combining the hourly RFC P with the most recent CAPE from NARR's 3-hourly reports. Here the R^2 values have jumped to as high as 30%; this is because the observed RFC precipitation is more accurate than the reanalyzed NARR precipitation. The dependence of R^2 on lag, however, is very similar to that in the left panel. Given these results, we henceforth use zero lag for the CAPE × P proxy; that is, we use contemporaneous CAPE and P.

4 CONUS-Integrated Time Series

One of the key results of R14 was the discovery of a high R^2 between the time series of CAPE × P and F over CONUS. To be more precise, let $\square X\square$ denote the area-weighted spatial integral of X over CONUS, for any variable X. R14 calculated $\square$CAPE$\square$ at 12-hourly intervals for the year 2011 from Stratosphere-troposphere Processes And their Role in Climate (SPARC) radiosonde data (SPARC, 2013). Likewise, $\square P\square$ and $\square F\square$ were calculated at 12-hourly intervals from RFC and NLDN, respectively. R14 found that the R^2 between the 12-hourly time series of $\square$CAPE$\square \times \square P\square$ and $\square F\square$ was 0.77 during the year 2011. Here we repeat this analysis using RRS instead of SPARC and calculate the R^2 over the 6-year period covering 2005 through 2010. The resulting R^2, which is given in the RRS-RFC entry of the $\square$CAPE$\square \times \square P\square$ block of Figure 2a, is 0.76, which is nearly identical to the value of 0.77 found by R14.

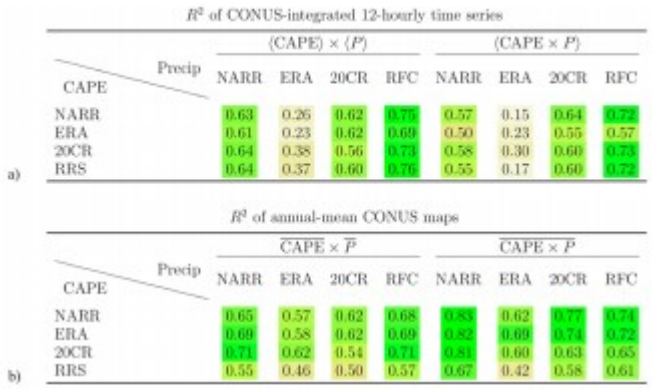

a)

R^2 of CONUS-integrated 12-hourly time series

CAPE \ Precip	⟨CAPE⟩ × ⟨P⟩ NARR	⟨CAPE⟩ × ⟨P⟩ ERA	⟨CAPE⟩ × ⟨P⟩ 20CR	⟨CAPE⟩ × ⟨P⟩ RFC	⟨CAPE × P⟩ NARR	⟨CAPE × P⟩ ERA	⟨CAPE × P⟩ 20CR	⟨CAPE × P⟩ RFC
NARR	0.63	0.26	0.62	0.75	0.57	0.15	0.64	0.72
ERA	0.61	0.23	0.62	0.69	0.50	0.23	0.55	0.57
20CR	0.64	0.38	0.56	0.73	0.58	0.30	0.60	0.73
RRS	0.64	0.37	0.60	0.76	0.55	0.17	0.60	0.72

b)

R^2 of annual-mean CONUS maps

CAPE \ Precip	$\overline{\text{CAPE}} \times \overline{P}$ NARR	$\overline{\text{CAPE}} \times \overline{P}$ ERA	$\overline{\text{CAPE}} \times \overline{P}$ 20CR	$\overline{\text{CAPE}} \times \overline{P}$ RFC	$\overline{\text{CAPE} \times P}$ NARR	$\overline{\text{CAPE} \times P}$ ERA	$\overline{\text{CAPE} \times P}$ 20CR	$\overline{\text{CAPE} \times P}$ RFC
NARR	0.65	0.57	0.62	0.68	0.83	0.62	0.77	0.74
ERA	0.69	0.58	0.62	0.69	0.82	0.69	0.74	0.72
20CR	0.71	0.62	0.54	0.71	0.81	0.60	0.63	0.65
RRS	0.55	0.46	0.50	0.57	0.67	0.42	0.58	0.61

Figure 2. (a) R^2 between 12-hourly (0 and 12 UTC) time series of CONUS CAPE × P from various combinations of data sources and the 12-hourly time series of CONUS lightning strike rate from NLDN. (b) R^2 between 0.5° (in both longitude and latitude) annual-mean CONUS maps of CAPE × P from various data sources and the 0.5° annual-mean CONUS map of lightning strike rate from NLDN. Darker greens correspond to higher R^2. UTC = universal time coordinated; CAPE = convective available potential energy; NLDN = National Lightning Detection Network; NARR = North American Regional Reanalysis; ERA = ERA-Interim; 20CR = twentieth Century Reanalysis version 2; RRS = Radiosonde Replacement System; RFC = River Forecast Centers.

Figure 2a shows the R^2 between 12-hourly (0 and 12 universal time coordinated [UTC]) NLDN F and either ⟨CAPE⟩×⟨P⟩ or ⟨CAPE × P⟩ from all possible combinations CAPE and P data sources. For each combination of CAPE and P data sources, the R^2 is calculated using the largest set of years that those data sources have in common with the NLDN data. The elements of Figure 2a are color coded such that greener cells correspond to higher correlations. Note that, for most combinations of data sources, ⟨CAPE⟩×⟨P⟩ and ⟨CAPE × P⟩ give very similar R^2. This means that there was little advantage to R14's method of spatially averaging CAPE and P separately before multiplying their time series; the time series of spatially averaged CAPE × P (i.e., ⟨CAPE × P⟩) works just as well.

Looking at the diagonal entries in Figure 2a (i.e., NARR-NARR, ERA-ERA, and 20CR-20CR), we see that NARR is the highest performing of the three reanalyses, giving 12-hourly R^2 of 0.63 and 0.57 for ⟨CAPE⟩×⟨P⟩ and ⟨CAPE × P⟩, respectively. Recalculating the R^2 at an hourly resolution to probe the reanalyses at times unconstrained by radiosonde data (see Text S3 for details and Table S1 for the results), we find that NARR is still the most accurate of the three reanalyses, with hourly R^2 of 0.63 and 0.60 for ⟨CAPE⟩×⟨P⟩ and ⟨CAPE × P⟩, respectively.

5 Time-Integrated CONUS Maps

Whereas Figure 2a and Table S1 give the temporal R^2 between CONUS-integrated time series, Figure 2b gives the spatial R^2 between annual-mean CONUS maps, all on a common 0.5° grid. Here for any variable X, we let $\overline{X}$ denote its time average. As before, we see that NARR gives the highest R^2: for $\overline{\text{CAPE} \times \text{P}}$ calculated from NARR CAPE and P, the spatial R^2 is 0.83. Note

also that the R^2 for NARR $\overline{\mathrm{CAPE} \times \mathrm{P}}$ (0.83) is greater than the R^2 for NARR $\overline{\mathrm{CAPE}} \times \overline{\mathrm{P}}$ (0.65) and that this inequality holds for all but a few of the data combinations. By capturing the temporal covariance between CAPE and P, $\overline{\mathrm{CAPE} \times \mathrm{P}}$ gives a more accurate picture of the spatial distribution of lightning.

From Figures 1 and 2b, we have learned that the best way to implement the CAPE × P proxy is to use contemporaneous and colocated values of CAPE and P, despite concerns about precipitation-driven downdrafts and their impact on CAPE. Fortunately, this is also the simplest way to implement the CAPE × P proxy in a weather or climate model: to predict the rate of flashes per area in a grid column, we simply take the product of that column's CAPE and P and multiply by an appropriate constant (found to be $\sim 10^{-11}$ J^{-1} by R14). We have also learned that, among the reanalyses, NARR gives the most accurate CAPE and P over CONUS, as quantified by the correlation of its CAPE × P with observed lightning flashes.

6 Seasonal and Diurnal Cycles

Having established contemporaneous and colocated CAPE × P as the optimal proxy and NARR as the best-performing reanalysis, we can apply this proxy to NARR data to examine the seasonal cycle of lightning maps over CONUS. The first four rows of Figure 3 show the seasonal maps of NARR $\overline{\mathrm{CAPE} \times \mathrm{P}}$ (left column) alongside the seasonal maps of NLDN $\overline{\mathrm{F}}$ (right column). The bottom row shows the annual means. In the left column, $\overline{\mathrm{CAPE} \times \mathrm{P}}$ has been normalized by a single multiplicative factor (7.8×10^{-12} J^{-1}) to convert from units of W m^{-2} to units of m^{-2} s^{-1}. While R14 showed that CAPE × P captures the time series of CONUS-integrated lightning, we see here that CAPE × P also largely captures the spatial distribution of lightning strikes and its seasonal variation. There are some discrepancies, of course, such as in the northern Gulf Coast and in Florida, where the proxy is about 50% too high. This may have to do with the relatively maritime character of the meteorology, which may cause the proxy to overpredict flash rates there as it does over the ocean (see section 7). Table S3 summarizes the spatial R^2 between seasonally averaged CAPE × P and seasonally averaged F for all combinations of data sources. For CAPE and P obtained from NARR, the R^2 values are 0.77 (December, January, February), 0.92 (March, April, May), 0.78 (June, July, August), 0.56 (September, October, November) and, as discussed in the previous section, 0.83 for the annual mean.

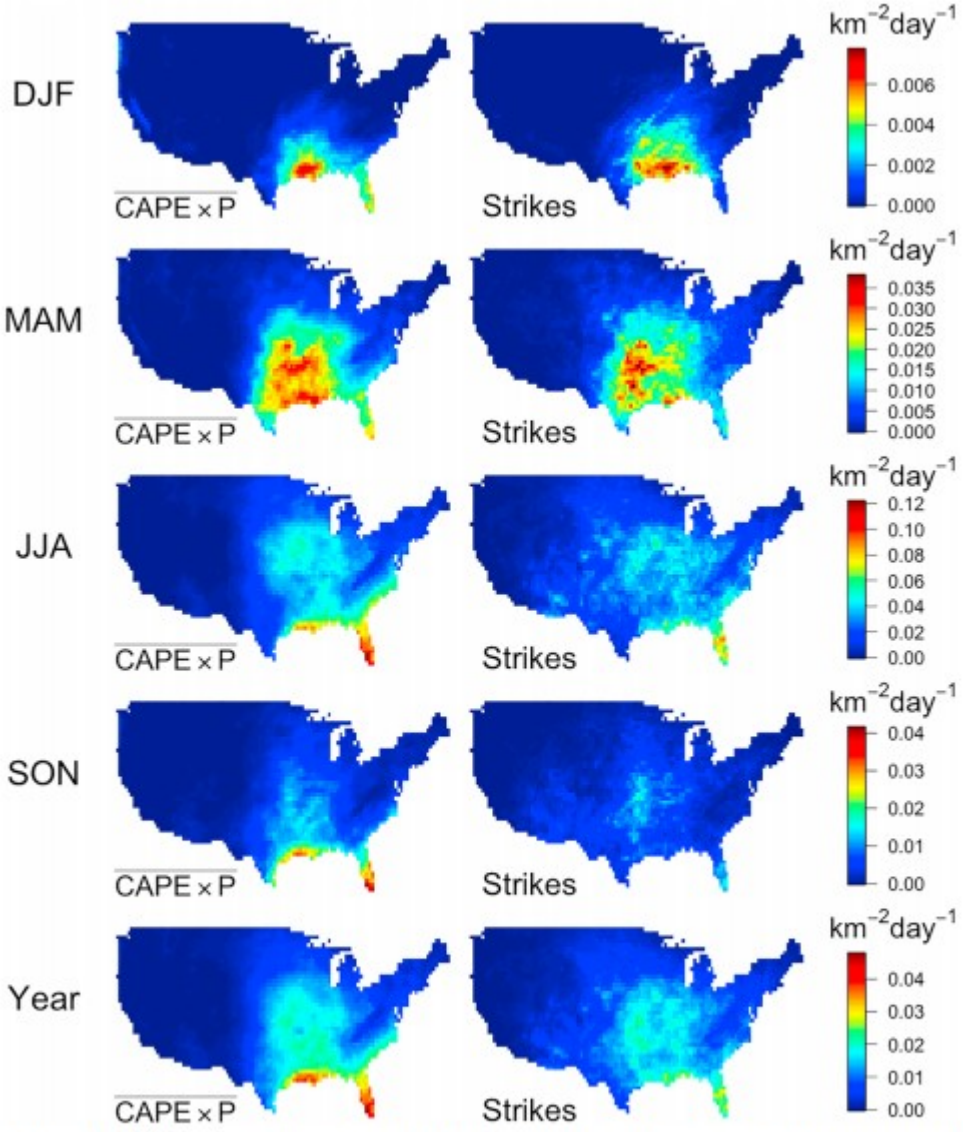

Figure 3. Maps of (left column) predicted and (right column) actual lightning for averages over four seasons and the entire year. The predicted lightning uses CAPE × P from NARR. CAPE = convective available potential energy; DJF = December, January, February; MAM = March, April, May; JJA = June, July, August; SON = September, October, November.

In R14, CAPE was calculated from 12-hourly radiosonde data. Because of that low temporal resolution, it was not possible to study the diurnal cycle of CAPE × P in any detail. Now, with the NARR data in hand, we can combine the 3-hourly NARR CAPE with the 1-hourly RFC P. The annually averaged diurnal cycle of CONUS-integrated CAPE × P, scaled by a single factor to give the observed mean strike rate, is shown as the blue curve at the top of Figure 4. Overlaid in red is the annually averaged diurnal cycle of CONUS-integrated F. We see that CAPE × P faithfully captures the shape, timing, and amplitude of the diurnal cycle in CONUS-integrated flash rate.

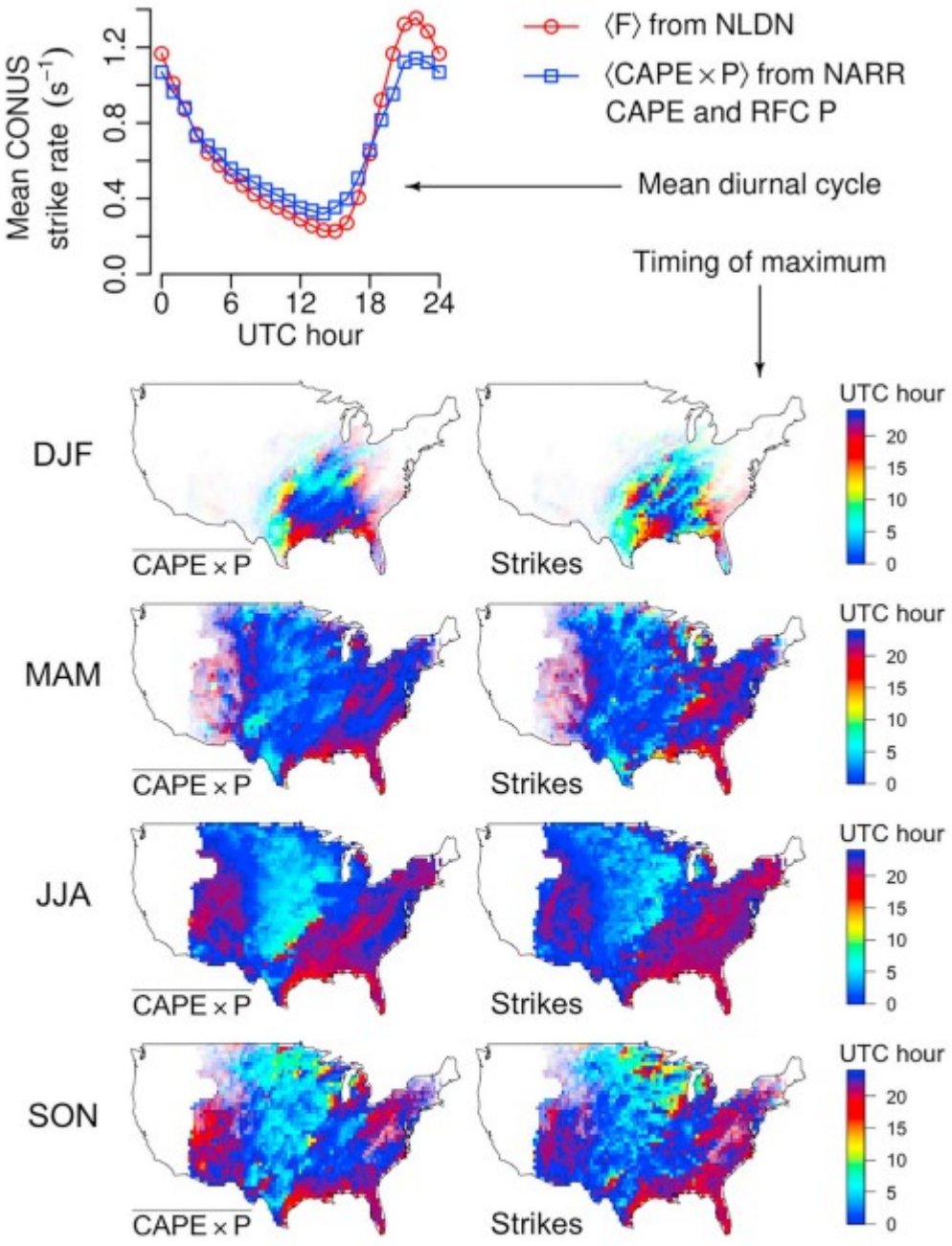

Figure 4. (top left) Annually averaged diurnal cycle of (red) CONUS-integrated cloud-to-ground lightning flash rate *F* and (blue) CONUS-integrated CAPE × P. (other panels) Hour UTC in which the (left column) predicted and (right column) actual flash rate maximizes, based on a sinusoid fit to the mean diurnal cycle. Diurnal cycles are averaged here over 2010–2015, inclusive. White areas indicate where there is no RFC data (western United States and parts of New England) and where the number density of flashes is too low to accurately reconstruct the diurnal cycle (colors are gradually masked to white for seasonal flash rates below 0.001 km^{-2} day^{-1}). CAPE = convective available potential energy; DJF = December, January, February; MAM = March, April, May; JJA = June, July, August; SON = September, October, November; UTC = universal time coordinated.

While the average diurnal cycle peaks at about 22 UTC, the timing of this peak varies with location and season. The maps in the right column of Figure 4 show the UTC hour of the maximal flash rate for each season,

calculated by fitting a sinusoid to the NLDN diurnal cycle and reporting the UTC hour of the peak of that sinusoid. From these plots, we see that most locations and times of the year have their peak flash rate within the 12 hr centered roughly on 0 UTC. The maps in the left column of Figure 4 show the peak hour of the CAPE × P proxy, calculated in the same way using the product of NARR CAPE and RFC P. By comparing the two columns, we see that CAPE × P captures the spatial and seasonal variations in the timing of the maximum flash rate with great fidelity.

7 Land-Ocean Contrast

Given these successes over CONUS, we might expect that CAPE × P performs well over land globally. Indeed, this is the case. Figure 5 shows the annual-mean lightning flash rate over land observed by LIS-OTD and WWLLN in the first row and the annual-mean $\overline{\mathrm{CAPE} \times \mathrm{P}}$ calculated from ERA and 20CR in the second row, all on logarithmic color scales spanning exactly three factors of 10. (Here the WWLLN data have been normalized to an effective flash rate as described in Text S1.) The correspondence between the two rows is quite good: CAPE × P applied to the reanalyses correctly predicts the largest flash rates in the Central United States, South America, Central Africa, South Asia, Southeast Asia, and Oceania. Although there are differences between the reanalyses and the observations, they are comparable to the differences between the two observational products.

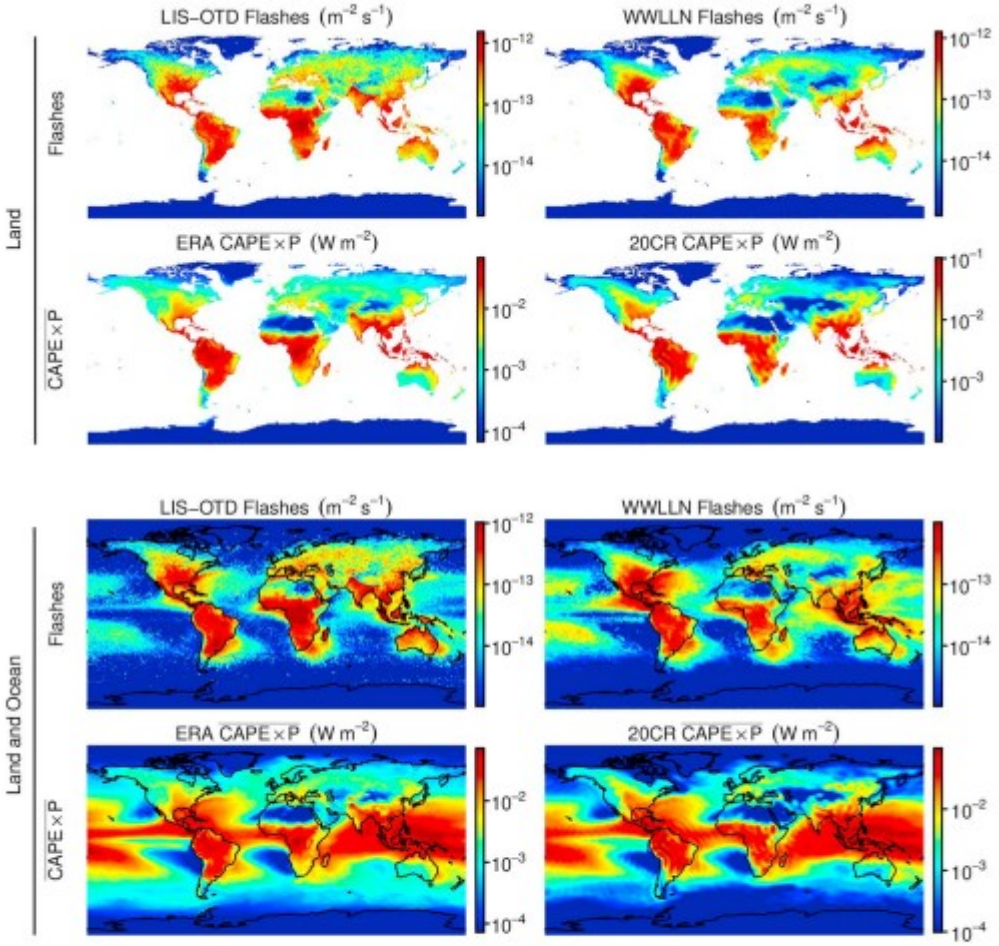

Figure 5. Annual-mean flash rate $\overline{F}$ from (first row, left) LIS-OTD and (first row, right) WWLLN and annual-mean $\overline{CAPE \times P}$ from (second row, left) ERA and (second row, right) 20CR. To draw attention to the land, the ocean is masked out in the top two rows. The bottom two rows are the same but with the ocean values plotted. LIS-OTD = Lightning Imaging Sensor and the Optical Transient Detector; WWLLN = World Wide Lightning Location Network; ERA = ERA-Interim; CAPE = convective available potential energy; 20CR = twentieth Century Reanalysis version 2.

It has long been recognized that the flash rate of maritime deep convection is much smaller than the flash rate of continental deep convection (Brooks, 1925; Cecil et al., 2014; Orville & Henderson, 1986). It is natural to speculate—perhaps even hope—that the differences in CAPE would explain the difference. Over land, the varied topography and the large diurnal cycle contribute to the occasional buildup of large CAPE, which is subsequently released in explosive convection. Over the ocean, where topography is absent and the diurnal cycle is damped by the high heat capacity of water, CAPE is much less variable. If precipitation were occurring primarily during high-CAPE events over land, then the CAPE × P proxy might naturally predict a large land-ocean contrast in lightning. Unfortunately, this is not the case. The bottom two rows of Figure 5 plot the same data as the top two rows but without the ocean data masked out. It is readily apparent that CAPE × P produces far too small a contrast between land and ocean flash rates. This

land-ocean contrast in lightning, and the failure of the CAPE × P proxy to predict it, is quantified in Text S4 and Figure S1. The mean rate of flashes per area over land is 9.1 (2.6) times higher than it is over the ocean in the LIS-OTD (WWLLN) data, but the mean land-ocean ratio of CAPE × P is 0.9 (0.9) in the ERA (NCEP) data. The failure of CAPE × P to explain the land-ocean lightning contrast means that some other factor is responsible. One candidate is the higher aerosol concentration over land; higher concentrations of aerosols have been shown to invigorate convection (Koren et al., 2005) and lead to higher flash rates (Stolz et al., 2015, 2017; Thornton et al., 2017). Another candidate is the lower relative humidity over land, which is associated with a deeper subcloud mixed layer and, therefore, cloudy updrafts that are wider at birth and, therefore, more protected from the buoyancy-sapping effect of convective entrainment (Lucas et al., 1994; Williams & Stanfill, 2002). Other factors that may contribute to the land-ocean contrast in lightning include the greater heterogeneity and topography of the land surface and the different shapes of updraft buoyancy profiles over land as compared to the ocean.

Acknowledgments

This work was supported by the U.S. Department of Energy's Atmospheric System Research program through the Office of Science's Biological and Environmental Research program under contract DE-AC02-05CH11231. Thanks are due to Katrina Virts for assistance with WWLLN data and to Steven Rutledge and an anonymous reviewer for their helpful feedback. The authors wish to thank the World Wide Lightning Location Network http://wwlln.net, a collaboration among over 50 universities and institutions, for providing the lightning location data used in this paper. The NARR data are available from NOAA at ftp://ftp.cdc.noaa.gov/Datasets/NARR/monolevel. The ERA data are available from ECMWF at www.ecmwf.int. The 20CR data are available from NOAA at ftp://ftp.cdc.noaa.gov/Datasets/20thC_ReanV2c/gaussian/monolevel. The RRS data are available from NOAA at ftp://ftp.ncdc.noaa.gov/pub/data/ua/rrs-data/. The LIS-OTD data are available from NASA at https://lightning.nsstc.nasa.gov/data/data_lis-otd-climatology.html. The RFC data are available by arrangement with W. Lawrence. The WWLLN data are available by arrangement with R. Holzworth. The NLDN data are available by arrangement with J. Molinari.

References

Brooks, C. E. P. (1925). The distribution of thunderstorms over the globe. *Geophysical Memoirs*, 24(3), 147– 164.

Cecil, D. J., Buechler, D. E., & Blakeslee, R. J. (2014). Gridded lightning climatology from TRMM-LIS and OTD: Dataset description. *Atmospheric Research*, 135, 404– 414.

Compo, G. P., Whitaker, J. S., Sardeshmukh, P. D., Matsui, N., Allan, R. J., Yin, X., Gleason, B. E., Vose, R. S., Rutledge, G., Bessemoulin, P., Brönnimann, S., Brunet, M., Crouthamel, R. I., Grant, A. N., Groisman, P. Y., Jones, P. D., Kruk, M. C., Kruger, A. C., Marshall, G. J., Maugeri, M., Mok, H. Y., Nordli, Ø., Ross, T. F., Trigo, R. M., Wang, X. L., Woodruff, S. D., & Worley, S. J. (2011). The twentieth century reanalysis project. *Quarterly Journal of the Royal Meteorological Society*, 137(654), 1– 28.

Cummins, K. L., & Murphy, M. J. (2009). An overview of lightning locating systems: History, techniques, and data uses, with an in-depth look at the US NLDN. *Electromagnetic Compatibility, IEEE Transactions on*, 51(3), 499– 518.

Dee, D. P., Uppala, S. M., Simmons, A. J., Berrisford, P., Poli, P., Kobayashi, S., Andrae, U., Balmaseda, M. A., Balsamo, G., Bauer, P., Bechtold, P., Beljaars, A. C. M., van de Berg, L., Bidlot, J., Bormann, N., Delsol, C., Dragani, R., Fuentes, M., Geer, A. J., Haimberger, L., Healy, S. B., Hersbach, H., Hólm, E. V., Isaksen, L., Kållberg, P., Köhler, M., Matricardi, M., McNally, A. P., Monge-Sanz, B. M., Morcrette, J.-J., Park, B.-K., Peubey, C., de Rosnay, P., Tavolato, C., Thépaut, J.-N., & Vitart, F. (2011). The ERA-Interim reanalysis: Configuration and performance of the data assimilation system. *Quarterly Journal of the Royal Meteorological Society*, 137(656), 553– 597.

Hutchins, M. L., Holzworth, R. H., Brundell, J. B., & Rodger, C. J. (2012). Relative detection efficiency of the World Wide Lightning Location Network. *Radio Science*, 47, RS6005. https://doi.org/10.1029/2012RS005049

Jacobson, A. R., Holzworth, R., Harlin, J., Dowden, R., & Lay, E. (2006). Performance assessment of the World Wide Lightning Location Network (WWLLN), using the Los Alamos Sferic Array (LASA) as ground truth. *Journal of Atmospheric and Oceanic Technology*, 23(8), 1082– 1092.

Kitzmiller, D., Miller, D., Fulton, R., & Ding, F. (2013). Radar and multisensor precipitation estimation techniques in National Weather Service hydrologic operations. *Journal of Hydrologic Engineering*, 18(2), 133– 142.

Koren, I., Kaufman, Y. J., Rosenfeld, D., Remer, L. A., & Rudich, Y. (2005). Aerosol invigoration and restructuring of Atlantic convective clouds. *Geophysical Research Letters*, 32, L14828. https://doi.org/10.1029/2005GL023187

Lucas, C., Zipser, E. J., & LeMone, M. A. (1994). Comments Convective available potential energy in the environment of oceanic and continental clouds: Correction and comments. *Journal of the Atmospheric Sciences*, 51(24), 3829– 3830.

Lucas, C., Zipser, E. J., & Lemone, M. A. (1994). Vertical velocity in oceanic convection off tropical Australia. *Journal of the Atmospheric Sciences*, 51(21), 3183– 3193.

Mach, D. M., Christian, H. J., Blakeslee, R. J., Boccippio, D. J., Goodman, S. J., & Boeck, W. L. (2007). Performance assessment of the optical transient detector and lightning imaging sensor. *Journal of Geophysical Research*, 112, D09210. https://doi.org/10.1029/2006JD007787

Mesinger, F., DiMego, G., Kalnay, E., Mitchell, K., Shafran, P. C., Ebisuzaki, W., Jovic, D., Woollen, J., Rogers, E., Berbery, E. H., Ek, M. B., Fan, Y., Grumbine, R., Higgins, W., Li, H., Lin, Y., Manikin, G., Parrish, D., & Shi, W. (2006). North American regional reanalysis. *Bulletin of the American Meteorological Society*, 87(3), 343– 360.

NCDC (2008). Data documentation for dataset 6213 (dsi-6213) (*Tech. Rep.*) 151 Patton Ave, Asheville, NC 28801-5001, USA: National Climatic Data Center.

Orville, R. E., & Henderson, R. W. (1986). Global distribution of midnight lightning: September 1977 to August 1978. *Monthly Weather Review*, 114(12), 2640– 2653.

Orville, R. E., & Huffines, G. R. (2001). Cloud-to-ground lightning in the United States: NLDN results in the first decade, 1989-1998. *Monthly Weather Review*, 129(5), 1179– 1193.

Romps, D. M. (2015). MSE minus CAPE is the true conserved variable for an adiabatically lifted parcel. *Journal of the Atmospheric Sciences*, 72(9), 3639– 3646.

Romps, D. M., & Kuang, Z. (2010). Do undiluted convective plumes exist in the upper tropical troposphere? *Journal of the Atmospheric Sciences*, 67(2), 468– 484.

Romps, D. M., Seeley, J. T., Vollaro, D., & Molinari, J. (2014). Projected increase in lightning strikes in the United States due to global warming. *Science*, 346(6211), 851– 854.

SPARC (2013). U.S. high vertical resolution radiosonde data. Retrieved from http://www.sparc-climate.org/data-center/data-access/us-radiosonde/

Stolz, D. C., Rutledge, S. A., & Pierce, J. R. (2015). Simultaneous influences of thermodynamics and aerosols on deep convection and lightning in the tropics. *Journal of Geophysical Research: Atmospheres*, 120, 6207– 6231. https://doi.org/10.1002/2014JD023033

Stolz, D. C., Rutledge, S. A., Pierce, J. R., & van den Heever, S. C. (2017). A global lightning parameterization based on statistical relationships among environmental factors, aerosols, and convective clouds in the TRMM climatology. *Journal of Geophysical Research: Atmospheres*, 122, 7461– 7492. https://doi.org/10.1002/2016JD026220

Thornton, J. A., Virts, K. S., Holzworth, R. H., & Mitchell, T. P. (2017). Lightning enhancement over major oceanic shipping lanes. *Geophysical Research Letters*, 44, 9102– 9111. https://doi.org/10.1002/2017GL074982

Virts, K. S., Wallace, J. M., Hutchins, M. L., & Holzworth, R. H. (2013). Highlights of a new ground-based, hourly global lightning climatology. *Bulletin of the American Meteorological Society*, 94(9), 1381– 1391.

Wacker, R. S., & Orville, R. E. (1999). Changes in measured lightning flash count and return stroke peak current after the 1994 U.S. National Lightning Detection Network upgrade: 1. Observations. *Journal of Geophysical Research*, 104(D2), 2151– 2157.

Williams, E., & Stanfill, S. (2002). The physical origin of the land-ocean contrast in lightning activity. *Comptes Rendus Physique*, 3(10), 1277– 1292.